PAPER

Check for updates

Surface functionalized silver-doped ZnO nanocatalyst: a sustainable cooperative catalytic, photocatalytic and antibacterial platform for waste treatment

Sagar Vikal,[a] Yogendra K. Gautam, [ID] *[a] Swati Meena,[b] Vijay Parewa, [ID] *[b] Ashwani Kumar,[c] Ajay Kumar,[d] Sushila Meena,[b] Sanjay Kumar[e] and Beer Pal Singh [ID] [a]

The different dyes used and discharged in industrial settings and microbial pathogenic issues have raised serious concerns about the content of bodies of water and the impact that dyes and microbes have on the environment and human health. Efficient treatment of contaminated water is thus a major challenge that is of great interest to researchers around the world. In the present work, we have fabricated functionalized silver-doped ZnO nanoparticles (Ag-doped ZnO NPs) via a hydrothermal method for wastewater treatment. X-ray photoelectron spectroscopy analysis confirmed the doping of Ag with ZnO NPs, and X-ray diffractometry analysis showed a decreasing trend in the crystallite size of the synthesized ZnO NPs with increased Ag concentration. Field emission scanning electron microscopy study of pure ZnO NPs and Ag-doped ZnO NPs revealed nanocrystal aggregates with mixed morphologies, such as hexagonal and rod-shaped structures. Distribution of Ag on the ZnO lattice is confirmed by high-resolution transmission electron microscopy analysis. ZnO NPs with 4 wt% Ag doping showed a maximum degradation of ~95% in 1.5 h of malachite green dye (80 mg L^{-1}) under visible light

[a]*Smart Materials and Sensor Laboratory, Department of Physics, Ch. Charan Singh University, Meerut 250004, Uttar Pradesh, India. E-mail: ykg.iitr@gmail.com*

[b]*Centre of Advanced Studies, Department of Chemistry, University of Rajasthan, Jaipur, India. E-mail: parewa@gmail.com*

[c]*Nanoscience Laboratory, Institute Instrumentation Centre, IIT Roorkee, Roorkee 247667, India*

[d]*Department of Biotechnology, Mewar Institute of Management, Ghaziabad 201012, Uttar Pradesh, India*

[e]*Department of Physics, University of Rajasthan, Jaipur 302004, India*

Mr. Sagar Vikal is a PhD scholar at the Department of Physics, Chaudhary Charan University (CCSU), Meerut, U.P., India, and received his M.Phil. (2019) from the same university. He has published three research papers in reputed journals, holds one Indian patent and contributed four book chapters to a book entitled "Green and Sustainable Nanotechnology" published by Springer in 2021. His research interests are focused on photocatalytic activity, antimicrobial activity, environmental remediation and gas sensors.

Dr Yogendra Kumar Gautam is working as an Assistant Professor at the Department of Physics, Chaudhary Charan University (CCSU), Meerut, U.P., India since 2015. He previously worked as an Assistant Professor at the Department of Physics, JUET Guna, M.P., India (2013–2015). He received his M.Tech. (Solid State Materials) at the Indian Institute of Technology (IIT) Delhi, India in 2007. He received his PhD (materials science) at IIT Roorkee, India in 2013. He has published 35 research articles in reputed journals and holds three national patents, and serves as a reviewer of several national/international journals of repute. His research activities are focused on gas sensors, hydrogen storage, energy storage devices, antimicrobial activity and photocatalytic activity.

and ~85% in 4 h under dark conditions. Up to five successive treatment cycles using the 4 wt% Ag-doped ZnO NP nanocatalyst confirmed its reusability, as it was still capable of degrading ~86% and 82% of the dye under visible light and dark conditions, respectively. This limits the risk of nanotoxicity and aids the cost-effectiveness of the overall treatment process. The synthesized NPs showed antibacterial activity in a dose-dependent manner. The zone of inhibition of the Ag-doped ZnO NPs was higher than that of the pure ZnO NPs for all doping content. The studied Ag-doped ZnO NPs thus offer a significant eco-friendly route for the effective treatment of water contaminated with synthetic dyes and fecal bacterial load.

1. Introduction

Water is a fundamental need and natural resource to enable the survival of living species on earth. Effects of climate change and population growth are globally linked to water pollution.[1] Synthetic dyes used in the paper and textile (clothing) industries are one of the major sources of pollution in water bodies.[2] Nowadays, these industries are witnessing a surge in the use of

Dr. Swati Meena is currently an Assistant Professor at the Department of Chemistry, University of Rajasthan, Jaipur, India. She completed her PhD in chemistry at Jai Narain Vyas University, Jodhpur, Rajasthan, India. She is the author and co-author of six scientific publications. Her main interests are waste water treatment, dye degradation and photocatalysis.

Dr. Vijay Parewa received his PhD from the University of Rajasthan (India) and continued his scientific education as a postdoctoral fellow with Prof. Anshu Dandia, FRSC. Currently, he is working as an assistant professor at the University of Rajasthan, Jaipur. He was honored as a "Member of Royal Society of Chemistry" (MRSC), London, and "Member of National Academy of Sciences" (MNASc), India. He has published 49 research papers and holds two national patents. His current research focuses on synthesizing advanced materials and exploring their applications in mild synthetic procedures in the frame of increasing interest in sustainable/green chemistry. Recently, his efforts have been directed to the development of visible-light-driven approaches for environmental remediation applications.

Dr. Ashwani Kumar has been working as a CSIR Pool Scientist at the Institute Instrumentation Centre IIT Roorkee, India since September 2020. He worked as a CSIR-Postdoctoral Research Associate at the Institute Instrumentation Centre (IIC), IIT Roorkee, India from September 2017 to September 2020. Dr Kumar earned a PhD degree in experimental condensed matter physics (nanoscience and nanotechnology) from IIT Roorkee, India, in April 2018. His research is focused on the fabrication and characterization of nanostructured thin films of novel and functional materials, and the study of their microstructural, optical, electronic, chemical sensing and electrochemical properties for photonics, optoelectronics, energy storage and solid-state sensing devices. He completed an M.Tech. in nanotechnology at IIT Roorkee, India, in 2013.
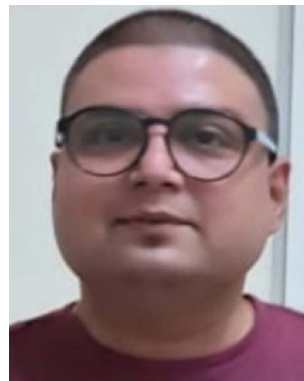
Ajay Kumar is currently an Assistant Professor at the Department of Biotechnology, Mewar Institute of Management, Vasundhara, Ghaziabad, U.P., India. He is a University Gold Medalist in M.Sc. Biotechnology. His areas of research interest are nanobiotechnology for agriculture and wastewater treatment applications, green chemistry, plant biochemistry and environmental biotechnology. He has published numerous articles in journals/magazines/proceedings/conference books.

organic dyes such as malachite green (MG).[3] These user-friendly dyes employed in the textile industry offer a diversity of colour palettes, stability, and extensive wet profiles.[4] However, the discharge of untreated water from such industries seriously threatens the environment and human health.[5] Dyes such as MG have carcinogenic, teratogenic, and mutagenic effects. There is ample literature available that mentions the consequences of dye-contaminated wastewater (MG, methylene blue (MB) and methyl orange (MO), *etc.*) on different parts of the environment.[6]

In addition to MG, *Escherichia coli* (*E. coli*) is a Gram-negative bacterial member of the fecal family coliform that normally lives in the intestines of humans and animals. *E. coli* is a strong indicator of sewage or animal waste pollution in water. Sewage and animal waste contain illness-inducing organisms. Consumption of such organisms causes serious illnesses, such as stomach upset, vomiting, fever or diarrhea.[7]

Fig. 1 Structure of MG dye.

The present study is focused on MG, which is an organic dye compound with a molecular weight of ~364.9 g mol^{-1} and represented by the molecular formula $C_{23}H_{25}ClN_2$[8]. MG is highly soluble in ethanol and water, forming blue-green solutions, and is widely used for dyeing materials such as paper, wool, leather, and cotton silk.[8] Moreover, this dye affects the reproductive and immune systems and shows potential genotoxic and carcinogenic effects.[9]

Many technologies have been established for the degradation of dyes as water pollutants, such as biodegradation, electrochemical, adsorption (physical), and chemical techniques.[10] Over the past few years, metal oxide NP-mediated photocatalysis under ultraviolet-visible (UV-vis) light has gained significant attention for degrading synthetic dyes in a wet environment.[11] Over conventional methods that require the use of harmful oxidants and/or facilitated partial dye degradation, photocatalysis offers an effective and eco-friendly route toward dye contamination instead of simply transforming the dye into another phase.[12] Photocatalysis is initiated by photons in UV light that excite electrons (e$^-$) in the valence band (VB) of the photocatalyst that then move to the conduction band (CB) and generate holes (h$^+$).[13] The generated e$^-$/h$^+$ pair promote reactions, which then leads to the complete reduction of organic pollutants, *e.g.*, dyes interact/adsorb on the surface of semiconductors.[14,15]

In the II–VI group, as a wide band gap semiconducting material, ZnO has attractive optical, electrical, sensing, catalytic, and magnetic properties.[16,17] The notable materialistic properties of ZnO have captivated scientific communities and

Prof. Beer Pal Singh received his M.Sc. (1997), M.Phil. (1998), and PhD (2002) from C.C.S. University, Meerut (UP), India. Presently, he is Professor and Head of the Department of Physics, CCS University, Meerut. He worked as a Visiting Professor at the Tokyo University of Science, Tokyo, Japan, and Visiting Scientist (Raman Fellow) at the University of Puerto Rico, Mayaguez, PR, USA. He has supervised nine PhD and more than 40 M.Phil. students. He has published more than 60 research papers in reputed journals, holds five national patents, and serves as a reviewer for several national/international journals of repute. His research interests are thin films, 2D materials, nanostructured materials, metal oxides, semiconducting materials, thin film transistors, sensors, environment remediation and energy storage devices.

Ms. Sushila Meena is currently doing research at the Department of Chemistry, University of Rajasthan, Jaipur, India. She completed her M.Sc. in chemistry at the Department of Chemistry, University of Rajasthan, Jaipur, India. Her research work is based on the synthesis and characterization of doped nanomaterials and their photocatalytic activity for wastewater treatment.
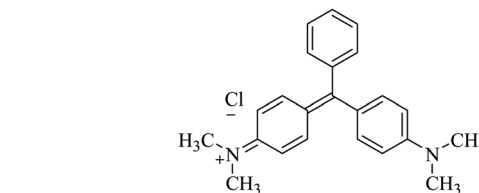
Dr. Sanjay Kumar received his PhD from the University of Rajasthan (India). Currently, he is working as an assistant professor at the Department of Physics, Rajasthan University, Jaipur, India. He received his M.Tech. (Solid State Materials) at the Indian Institute of Technology (IIT) Delhi, India, in 2007. He has published 20 research papers. His current research focuses on strongly correlated electron systems (experimental) and perovskite oxide thin films, as well as spintronic devices.

driven research on ZnO at the nanoscale level because of its application in sensors, photocatalysis, biological screening, cosmetics, electronics, and optoelectronics.[18] In the search for ZnO NPs with novel properties, doping with metals is a promising area where surface properties can be fine-tuned based on the target applications.[19] Several research groups, such as Vikal *et al.*,[10] Ikram *et al.*,[20] Mishra *et al.*,[21] Ambedkar *et al.*,[15] Kadhim *et al.*,[22] Zelekew *et al.*,[17] Liu *et al.*,[1] and Kumar *et al.*,[23] have prepared ZnO NPs doped with different metals, such as silver (Ag), copper (Cu), chromium (Cr), manganese (Mn), aluminium (Al) and magnesium (Mg), *etc.*, *via* diverse approaches. However, the selection of dopants is based on the type of application coupled with the methodology adopted. Many researchers have performed ZnO NP doping with different noble metals, such as Ag, Au, Pd, and Pt, for enhanced photocatalytic activity.[24] Among other noble metals, Ag has been identified as a suitable candidate for catalytic activities because of its high electrical conductivity, non-hazardous nature, stability, and relative affordability among materials.[25–28] Silver is seen as a preferred dopant for creating shallow acceptor levels in the ZnO lattice and is an appropriate candidate for photocatalytic and various optical applications. The benefits of Ag as a dopant in a ZnO lattice enhanced superficial charge delivery and CB generation *via* a photocatalytic reaction when it exposed to UV light.[28]

To the best of available resources, there has been no significant literature reported so far that has examined the photocatalytic reduction of MG dye under dark conditions using Ag-doped ZnO NPs.

Therefore, the present work is focused on the preparation of functionalized Ag-doped ZnO nanocatalysts for the treatment of waste contaminated with MG dye and fecal coliform bacteria, *i.e.*, *E. coli* (Fig. 1).

2. Experimental

2.1 Materials and methods

The MG dye, zinc chloride ($ZnCl_2$), silver nitrate ($AgNO_3$), sodium hydroxide (NaOH), hydrochloride acid (HCl), benzoquinone, *tert*-butanol and ammonium oxalate chemicals used in the experiments were of analytical grade and utilized as such without any further purification. All solutions used in the experimental work were prepared in double-distilled water (DDW).

2.2 Synthesis of pure and Ag-doped ZnO NPs

ZnO NPs were prepared *via* a chemical route (hydrothermal synthesis) utilizing $ZnCl_2$ (0.7 M) as a precursor salt and an aqueous solution of NaOH (1 M) as a precipitating agent.[29] The reaction mixture was allowed to process in an autoclave at 210 °C temperature for 8 h under autogenous pressure.[29] The ZnO-NPs were recovered as a white precipitate following filtration, washed multiple times with DDW, allowed to dry at 140 °C for 120 min,[29] and finally adopted a fine powdered form. Similar steps were undertaken to synthesize Ag-ZnO-NPs by varying the dopant ($AgNO_3$) concentration to obtain ZnO NPs with 2%, 4%, and 6% Ag doping (wt%).[30] The prepared Ag-doped ZnO samples were annealed at 800 °C for 180 min.[31] Fig. 2 shows the important steps in fabricating undoped and Ag-doped ZnO NPs *via* hydrothermal synthesis. The detailed process, including the chemical reactions involved at each synthesis stage, is provided in our previous study.[10]

2.3 Characterization of pure and Ag-doped ZnO NPs

The structure, phases, and crystallinity of the synthesized ZnO NPs were analysed using an X-ray diffractometer (Bruker AXS, D8 Advance). Field emission scanning electron microscopy (FESEM) (FEI, Quanta 200F) and energy dispersive X-ray (EDX) analysis were used to examine the surface morphology and composition of the ZnO NPs, respectively. The structural and morphological properties of the Ag-doped ZnO NPs were confirmed through transmission electron spectroscopy (TEM) measurements. X-ray photoelectron spectroscopy (XPS) was performed to analyse the electronic spectra of Ag and confirm the doping of the ZnO lattice. UV-vis and photoluminescence spectroscopies were used to evaluate the optical properties and chemical bonding of the prepared Ag-doped ZnO NPs, respectively.
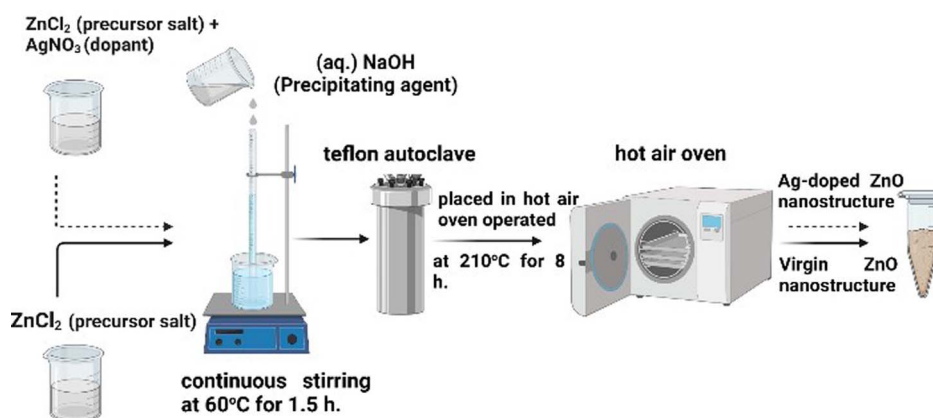

Fig. 2 Schematic diagram of the synthesis of pure and Ag-doped ZnO NPs.

2.4 Photocatalytic activity

Aqueous solutions of the dye were prepared in DDW (80 mg L^{-1}), using 5 mg of the respective ZnO NPs or Ag-doped ZnO NPs (Ag concentration varied from 2–6%) as a catalyst, followed by continuous stirring in a double-walled quartz photoreactor equipped with a water chiller and a 35 W tungsten lamp as a light source.[32] At 15 min time intervals, a 5 mL aliquot from each treatment was collected, centrifuged at 10 000 rpm, and the absorbance of the supernatant was recorded at 617 nm using UV-vis spectroscopy.[33] The effects of dye concentration (60–140 mg L^{-1}), pH (6 to 10), and dark conditions on the degradation of MG dye were also investigated for the optimized catalyst treatment. The degradation rate was calculated using eqn (1):

$$\eta = \frac{A_0 - A_t}{A_0} \times 100\% \tag{1}$$

where A_0 and A_t are the initial absorbance and absorbance at time "t", respectively.[21]

2.5 Antimicrobial activity of the Ag-doped ZnO NPs

The antibacterial activity of the pure ZnO and Ag-doped ZnO NPs was tested against *E. coli* by agar disc diffusion assay (ADDA), which is commonly used for microbial sensitivity testing.[34] A pure culture of *E. coli* was inoculated into freshly prepared nutrient Broth media and maintained at 37 °C for ~16 h.[35] After ~16 h, the *E. coli* cell culture (10 μL) was spread on solidified nutrient agar media in Petri dishes. Sterile filter paper discs (~6 mm each)[36] dipped in different concentrations of NPs (0 to 1000 ppm)[37] were placed on Petri dishes. The discs dipped in DDW were considered to be a negative control.[38] The Petri dishes were kept in an incubator overnight, and the zone of inhibition (ZOI) was recorded in mm.

3. Results and discussion

3.1 Structural properties

The diffraction peaks (Fig. 3) of pure ZnO NPs and Ag-doped ZnO NPs were observed at 2θ values of 31.88°, 34.59°, 36.34°, 47.68°, 56.78°, 63.07°, 68.05°, and 69.36°, corresponding to (100), (002), (101), (102), (110), (103), and (112) orientations, respectively [JCPDS card number 36-1451].[21,22] A highly intense peak was observed at 36.34° for the (101) lattice plane. The XRD analysis of the Ag-doped ZnO NPs revealed a reflection at 46.32° corresponding to Ag$_2$O along the lattice plane (211) [JCPDS card number 76-1393].[22,23]

The Scherrer equation was used to estimate the crystallite size (CS) of the prepared NPs for a highly intense peak (eqn (2)).[39,40] Where, D is the average crystallite size, λ is the CuK$_\alpha$-radiation (0.154 nm), β full width at half maximum (FWHM) of the peak, and θ is the Bragg's angle. It was observed that the CS decreased with an increase in Ag concentration, *i.e.*, in the order of: ZnO NPs (42 nm) > 2 wt% Ag-doped ZnO NPs (40 nm) > 4 wt% Ag-doped ZnO NPs (38 nm) > 6 wt% Ag-doped ZnO NPs (36 nm).
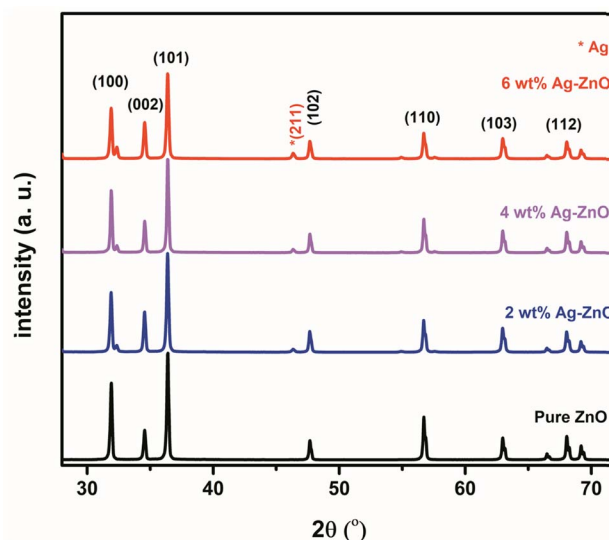

Fig. 3 XRD patterns of pure and Ag-doped ZnO NPs.

$$D = \frac{0.89\lambda}{\beta \cos\theta} \tag{2}$$

Such variations in the CS of prepared NPs could be due to the fact that the ionic radius of Ag (0.126 nm) is far greater than that of Zn (0.074 nm).[41] The observed peak of Ag$_2$O in the XRD patterns clearly indicated the formation of crystalline Ag clusters in the nanostructures.[17] Similar to other monovalent dopants like Na$^+$ and K$^+$, Ag occupied both the lattice and interstitial sites.[41]

3.2 Surface and elemental analysis

Fig. 4 shows FESEM images that reveal the mixed hexagonal and rod-shaped morphologies of the pure ZnO and Ag-doped ZnO nanocrystal aggregates. Nie *et al.*[42] reported the formation of rod-shaped ZnO NPs *via* a hydrothermal method. The elemental composition of the synthesized NPs from EDX analysis confirmed the presence of Ag, Zn, and O in suitable stoichiometric proportions.[42]

3.3 XPS analysis

XPS measurements were carried out for undoped and Ag-doped ZnO NPs. The binding energies of each element were calibrated using C 1s. Fig. 5(a)–(c) show the evolution of the XPS spectra as a function of increasing Ag dopant content corresponding to the Zn, Ag, and O elements, respectively. In Fig. 5(a), the peaks at ~1021.69 and ~1044.79 eV binding energies correspond to the Zn 2p$_{3/2}$ and Zn 2p$_{1/2}$ states, respectively. Fig. 5(b) shows the Ag XPS spectra and the peak positions at ~367.19, and ~373.23 eV binding energies were attributed to the Ag 3d$_{5/2}$ and Ag 3d$_{3/2}$ states, respectively. Interestingly, we observed that the peak positions showed a subtle shift toward a lower binding energy as the value of the Ag dopant increased.[43] Fig. 5(c) shows the O 1s spectra featuring a peak at ~530.27 eV and a broad tail-like
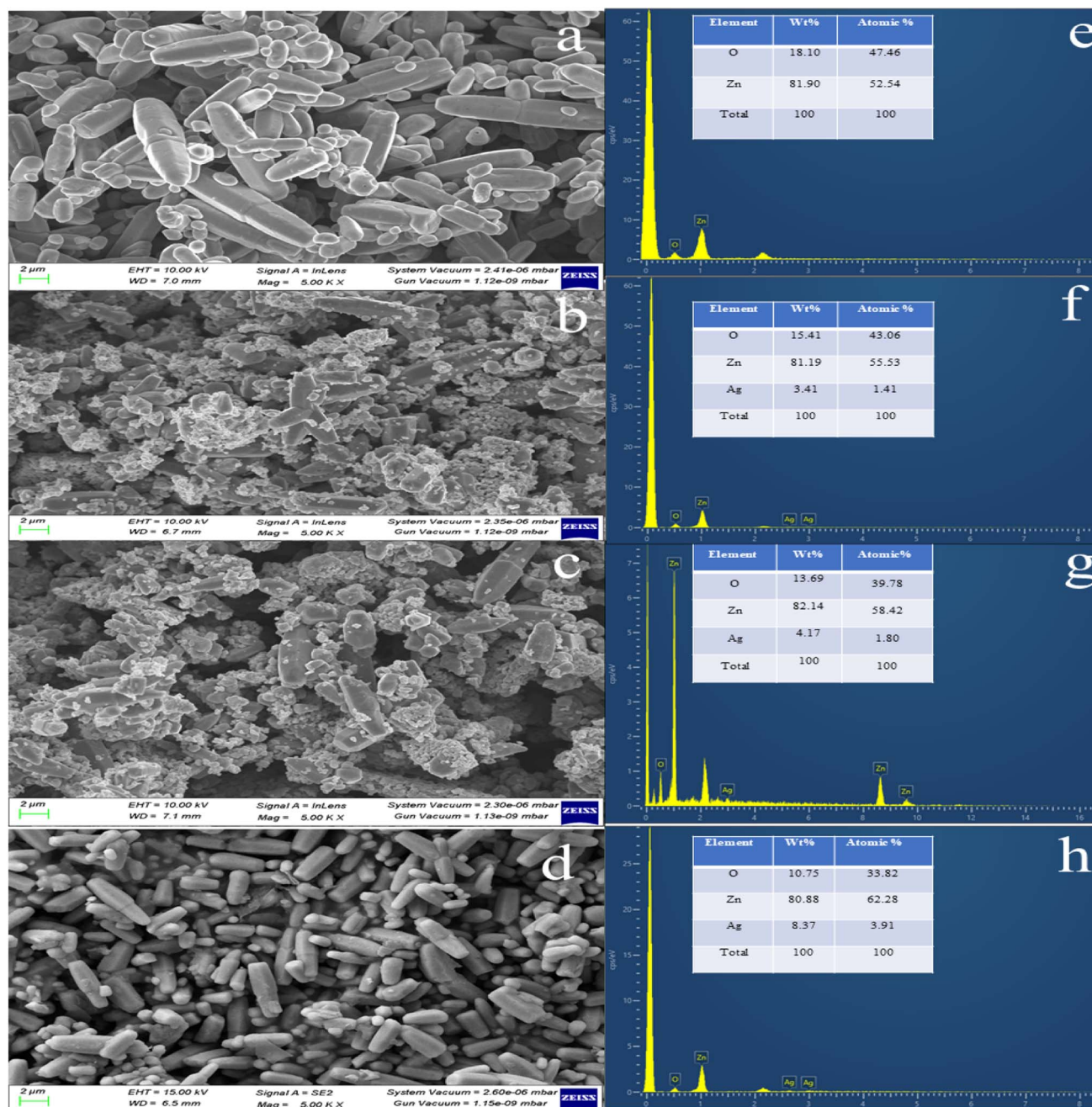
Fig. 4 FESEM with an EDX image of (a and e) pure ZnO, (b and f) 2 wt% Ag-doped ZnO NPs, (c and g) 4 wt% Ag-doped ZnO NPs, and (d and h) 6 wt% Ag-doped ZnO NPs.

feature due to oxygen defects at a higher binding energy. As such, there was no significant change in the peak position with an increase in Ag doping. We can state here that the Ag dopant is appropriately integrated within the ZnO lattice, which may cause defects and chemical shifts, which can be easily probed *via* photoluminescence (PL) spectral analysis.

3.4 UV-vis spectroscopy analysis

The absorption spectra of pure and Ag-doped ZnO NPs were obtained at room temperature using a UV-vis

spectrophotometer. The Tauc equation[44] was used to calculate the energy band gap of pure and Ag-doped ZnO NPs.

$$(\alpha h\nu)^n = B(h\nu - E_g) \tag{3}$$

where α, $h\nu$, E_g, and B are the absorption coefficient, photon energy, band gap energy, and a constant, respectively. The value of the index 'n' was calculated to be 2 from a Tauc plot (Fig. 6). Band gaps of 3.20 eV, 3.18, 3.15, and 3.13 eV were determined for pure ZnO and the 2, 4, and 6 wt% Ag-doped ZnO NPs, respectively. It was noted that the band gap decreased with an increase in the concentration of Ag in ZnO.[45] A red shift was
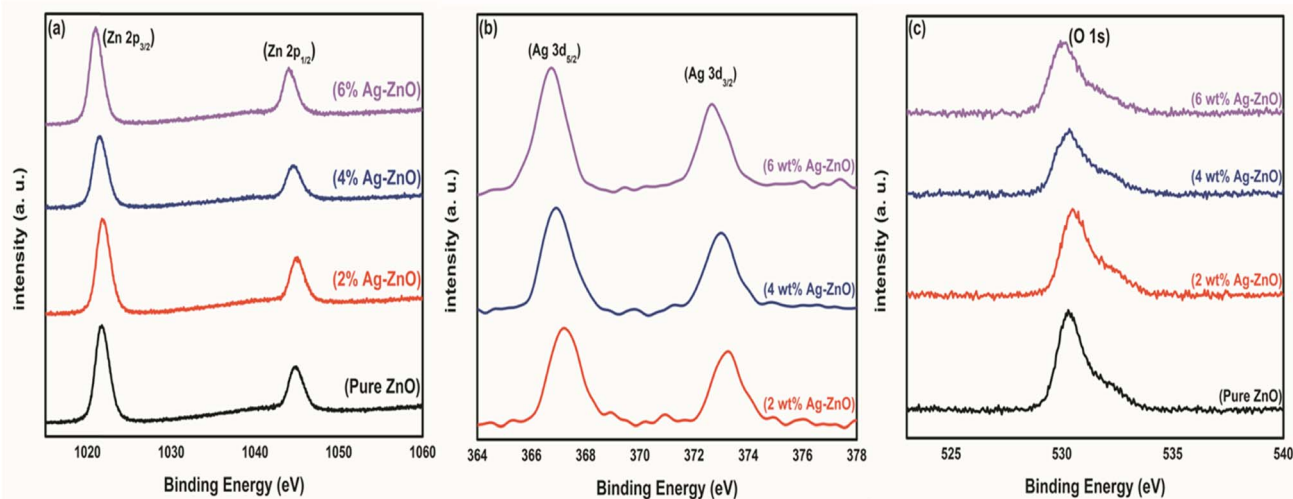
Fig. 5   (a) Zn 2p, (b) Ag 3d, and (c) O 1s XPS analysis.
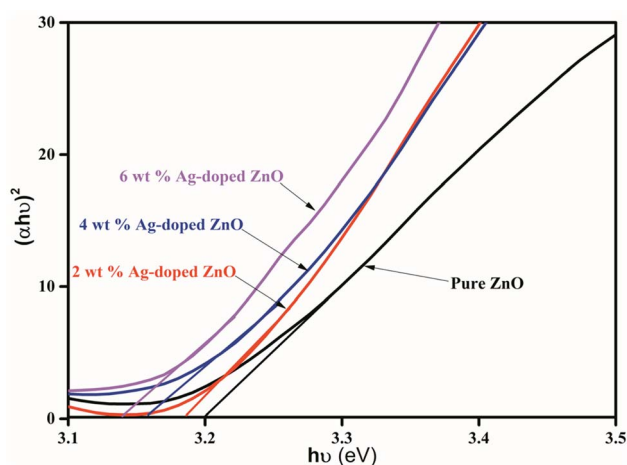

Fig. 6   Energy band gap diagram (Tauc plot) for pure and Ag-doped ZnO NPs.

observed in the band gap upon increasing the doping concentration of Ag in the Ag-doped ZnO NPs. This may be due to intermediate levels forming between the CB and VB of the host ZnO matrix.[46] Ag atoms play an important role as an acceptor to decrease the band gap of ZnO NPs.[23,45,47] Therefore, the variation in energy band gap of Ag-doped ZnO NPs has potential applications in photocatalysis.[48]

3.5   PL spectroscopy analysis

The PL spectra of pure ZnO NPs and Ag-doped ZnO NPs are shown in Fig. 7. The ZnO NPs typically exhibit two emission bands, i.e., in the UV and visible regions. In the UV region, the band with a peak at 360 nm is due to the near band edge (NBE) emission owing to free exciton recombination.[49] The second emission band is in the visible region (423 nm), which can be attributed to the recombination of an electron–hole pair. In addition to this, intrinsic point defects formed such as zinc

interstitials, antisite oxygen, oxygen and zinc vacancies, and the inclusion of hydroxyl groups in the crystal lattice through a growth process.[10] The peak at 423 nm in the PL spectra of the Ag-doped ZnO NPs samples was attributed to defects in the ZnO lattice.[50] Due to these defects, there are e^- transitions between the Zn vacancies and O interstitial states.[51] The position of the UV band is unchanged an increase in Ag doping, while its intensity decreased due to the interactions between the Ag dopant and ZnO NPs at grain boundaries.[51] This relationship decreased the e^-–h^+ recombination induced by UV light irradiation and improved the photocatalytic action.[51] The reduction in intensity of UV band was due to the formation of Ag atoms (interstitial position) at the ZnO lattice by producing many defects.[52] Ag^{2+} ions can bind into the ZnO matrix in two ways: replacing Zn^{2+} ions by producing doubly-ionized oxygen spaces or combining them as interstitials.[53] So, the intensity of the UV-vis band for ZnO NPs is decreased after substitution of ≤4 wt% Ag atoms in Zn lattice and then donated two electrons during
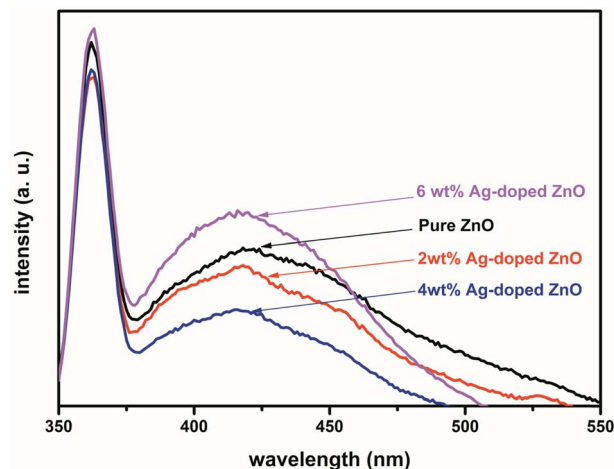

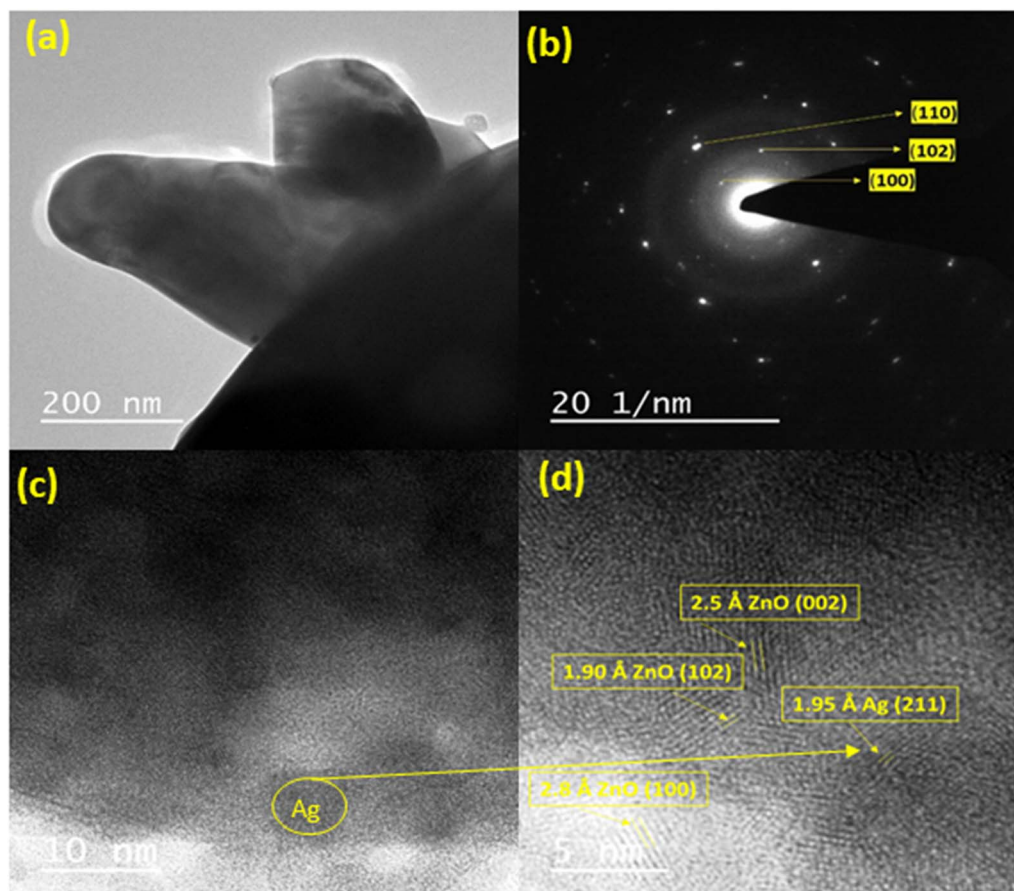Fig. 7   PL spectra of pure and Ag-doped ZnO NPs.

Fig. 8 TEM and HRTEM images. (a) TEM image of the 4 wt% Ag-doped ZnO NPs, (b) SAED pattern of the 4 wt% Ag-doped ZnO NPs, (c) HRTEM image of the 4 wt% Ag-doped ZnO NPs and (d) interplanar lattice spacing in the 4 wt% Ag-doped ZnO NPs.

band creation and shifted charge from Ag^{2+} to the VB, resulting in photoluminescence.[53] For the ≥ 6 wt% Ag-doped ZnO, an excess of Ag^{2+} ions were generated interstitially, producing lattice defects and rising peak intensity in the spectra with a further increase in Ag doping.[52] At a high percentage of Ag, its atoms accumulate in the form of Ag_2O, as observed from the XRD data. Ag as a dopant in the ZnO lattice therefore dictates the intensity (decrease/increase) of photoluminescence.[52]

3.6 Transmission electron microscopy (TEM) analysis

Fig. 8(a) shows the TEM images of 4 wt% Ag-doped ZnO NPs, in which a uniform distribution of Ag is observed on the surface of the ZnO lattice without any aggregations.[54] The selected area electron diffraction (SAED) pattern of 4 wt% Ag-doped ZnO NPs is shown in Fig. 8(b), which clearly shows the random scattering of diffraction spots along with a ring pattern, indicating the polycrystalline nature of the Ag-doped ZnO NPs. Distribution of Ag on the ZnO lattice was confirmed from the HRTEM images shown in Fig. 8(c) and (d). The interplanar lattice spacing (d) values were measured as 2.5 Å, 1.90 Å and 2.8 Å, corresponding to the (002), (102) and (100) planes, respectively, for ZnO, while that of 1.95 Å was attributed to the (211) plane of silver. These planes were also observed in the XRD analysis.

3.7 Photocatalytic degradation study

3.7.1 Effect of dopant concentration. The photocatalytic activity of pure and Ag-doped ZnO NPs was evaluated from the degradation of MG dye. The primary reaction parameters like dye concentration (80 mg L^{-1}), catalyst loading (5 mg/50 mL of dye solution), and pH (neutral) were fixed for the screening of the best catalysis of different fabricated NPs. The degradation rate of MG dye was observed through absorbance data (OD at 617 nm) recorded from UV-vis spectroscopy.

Table 1 Degradation of MG dye using different catalysts under dark and light conditions[a]

Catalyst used	Contact time (hours)	Dye degradation rate (%)
—	2	5
ZnO NPs (5 mg)[b]	2	6
2% Ag-doped ZnO NPs[b]	20	50
4% Ag-doped ZnO NPs[b]	1.5	95
6% Ag-doped ZnO NPs[b]	1.5	87
4% Ag-doped ZnO NPs[c]	4	85

[a] Catalysis was achieved at a dye concentration of 80 mg L^{-1}, catalyst loading of 5 mg, pH = 7 under (b) visible light and (c) dark conditions.

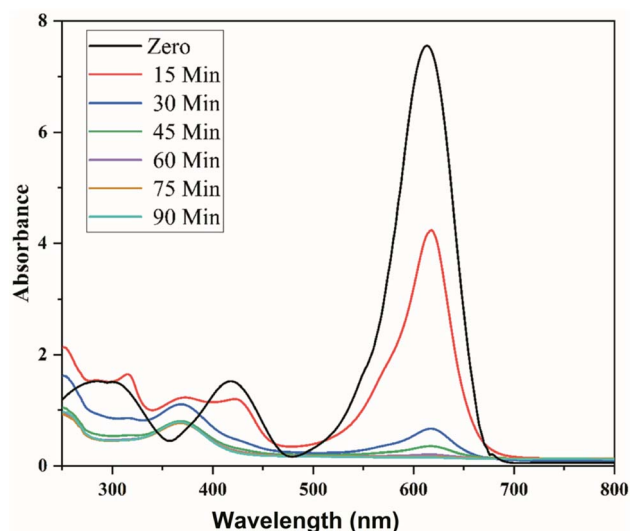Fig. 9 Time-dependent UV-vis absorption spectra of MG dye catalysed by 4 wt% Ag-doped ZnO NPs.

Fig. 10 Effect of concentration the degradation of dye catalysed by the 4 wt% Ag-doped ZnO NPs.

Table 1 shows a negligible change in dye solution without catalyst loading, while pure ZnO NPs showed only 6% of dye degradation under visible light, which could be due to its large band gap. About 50% dye degradation was achieved in 20 h utilizing the 2% Ag-doped ZnO NPs as a photocatalyst. Further, the 4 wt% Ag-doped ZnO NPs degraded up to 95% of the MG dye solution within 1.5 h. Fig. 9 shows the time-dependent UV-vis absorption spectra of MG dye catalysed by the 4 wt% Ag-doped ZnO NPs. A further increase in dopant concentration (6% Ag) resulted in ~87% dye degradation in 1.5 h. Doping of Ag in the pure ZnO NPs increased the photocatalytic activity and created a Fermi level, which was lower than the CB of ZnO, decreasing the band gap of ZnO, and Ag ions substituted for Zn^{2+} or interstitial positions, creating more lattice defects and resulting in Schottky barrier properties.[51,52] Overall, maximum dye degradation under visible light conditions was achieved with the 4 wt% Ag-doped ZnO NPs. A comparison of the present
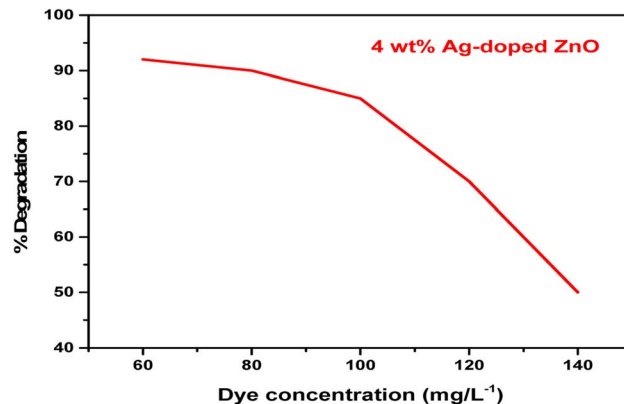
work with other reports based on different metal oxide catalysts is given in Table 2.

Furthermore, remarkable results were also obtained under dark conditions for 4 wt% Ag-doped ZnO as it degrades ~85% of the dye solution. These results show the potential utility of the Ag-doped ZnO NPs as a catalyst for effective dye degradation under dark conditions. Under dark conditions, the catalytic activity of the Ag-doped ZnO NPs may arise due to various oxygen defects. These defects were confirmed by PL analysis.[52]

3.7.2 Effect of Mg dye concentration. The photocatalytic activity of 4 wt% Ag-doped ZnO NPs at different dye concentrations (60 mg L^{-1} to 140 mg L^{-1}) was studied. The reaction parameters, such as catalyst load (5 mg), pH (neutral), and operation temperature (RT) were fixed. It was observed that the rate of degradation decreased with an increase in dye concentration (Fig. 10). This observation can be explained by two possibilities. Firstly, an increase in the dye concentration resulted in the absorption of the increasing number of dye molecules on the surface of the Ag-doped ZnO NPs. Consequently, a lower amount of reactive oxygen species (ROS, OH^-) and h^+ are available for the photocatalytic degradation of an

Table 2 Comparison between the previous and present results of catalysts under dark and light conditions

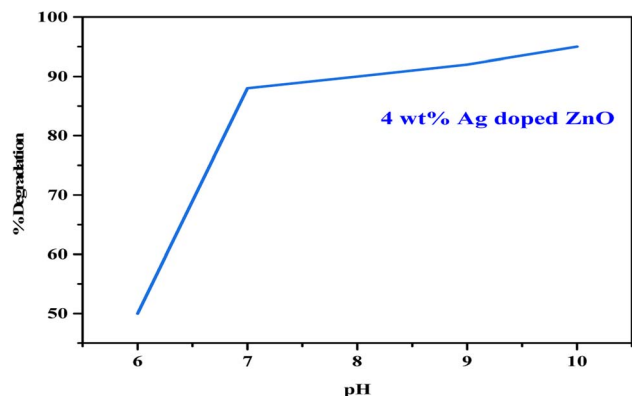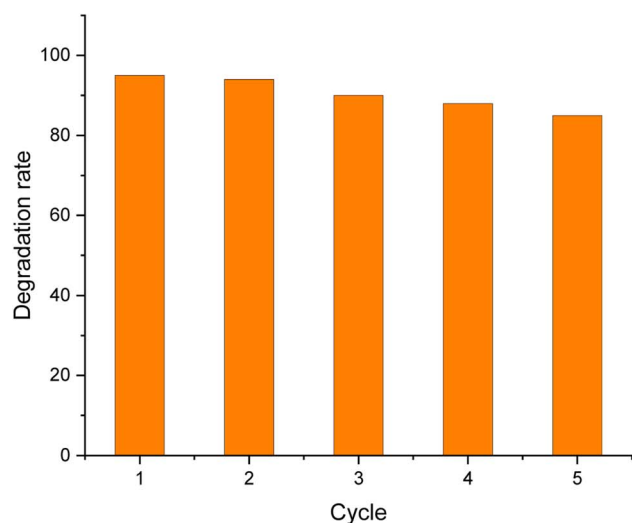| Catalysts | Degradation result (%) under an irradiation source | | Dye | Duration (min) | Reference |
	Dark	Visible			
NiO	—	89	MG	120	55
Ag$_2$O	—	94	MG	240	56
CuO	—	88	MG	160	57
FeO	—	88	MG	60	58
Co-doped TiO$_2$	—	82	MG	120	59
Pd/N-TiO$_2$	—	75	MG	90	60
PANI/ZnO	20	99	MG	300	61
Chitosan/TiO$_2$	—	92	MG	240	62
Graphene-CdO/SnO$_2$	—	94	MG	120	63
Ag-doped ZnO	—	**95**	**MG**	**90**	**Present work**
	85	—	MG	240	

Fig. 11 Effect of pH on the 4 wt% Ag-doped ZnO NPs.

(a)
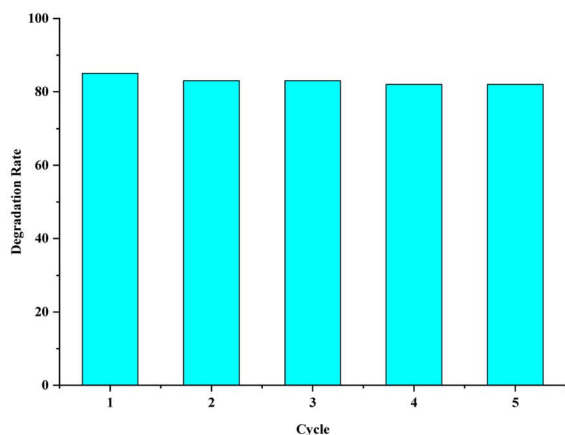
(b)

Fig. 12 Reusability of the catalyst under (a) visible light and (b) dark conditions.

increasing number of dye molecules. Secondly, visible light absorbed by the dye molecule may not reach the NP matrix, diminishing the degradation rate of highly concentrated dye solution.[54,64] Hence, the generation of intermediates increased, and the number of side reactions also competed with the dye degradation.

3.7.3 Effect of catalyst load. The amount of photocatalyst also affects the degradation rate of the dye, as it was observed in several experiments by varying the photocatalyst load from 1 to 5 mg (at pH = 7 and dye concentration = 80 mg L^{-1}). The dye degradation is increased with an increase of catalyst (4% Ag-doped ZnO NPs) load due to the availability of a high surface area and large number of active sites for the photo-degradation.[53] However, an excess amount of photocatalyst might induce high aggregation, affecting the availability of the photocatalyst surface area and thereby decreasing the rate of degradation.[52,64,65]

3.7.4 Effect of pH. The dye degradation was found to be affected by pH in the presence of a photocatalyst.[66] We observed an increase in the dye degradation potential of the 4% Ag-doped ZnO NPs with an increase in pH (6 to 10) while keeping the other parameters constant (Fig. 11). The pH of the dye solution affected the surface charge properties and size of the photo-catalyst aggregates, as well as the availability of hydroxyl groups to the photocatalyst.[67] A good degradation rate (95%) was observed at pH = 8 under light (~90 min) and dark conditions (~240 min).

3.7.5 Reusability of the photocatalyst. We also investigated the photocatalytic and catalytic potential of the synthesized NPs (4 wt% Ag-doped ZnO NPs) in terms of their reusability in successive treatment cycles. After every cycle, the recovered photocatalyst and catalyst were able to degrade ~86% and 82% of the dye under visible light and dark conditions, respectively. However, after the 5th run, a reduction in photocatalytic and catalytic performance was noticed in all the experimental trials (Fig. 12).
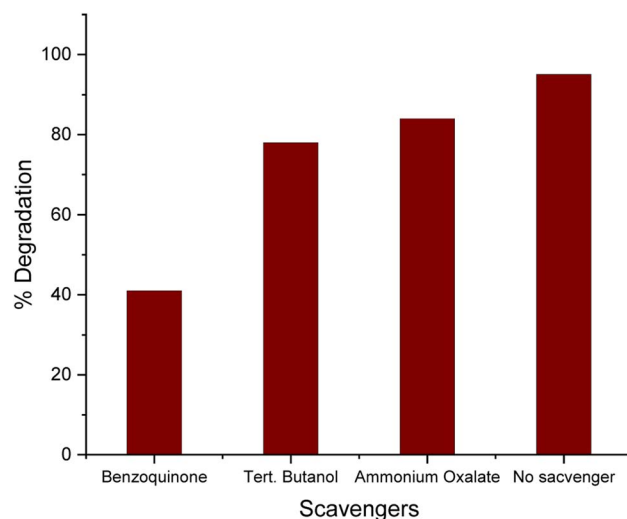

Fig. 13 Role of radical scavengers in the photodegradation of MG dye.

3.7.6   Role of ROS in the MG dye degradation. The use of scavengers is one of the critical parameters by which to identify the active species responsible for the photocatalytic degradation of dye. In this experiment, different scavengers, such as *tert*-butanol (TB), ammonium oxalate (AO), and benzoquinone (BQ), were used to monitor the role of hydroxyl radicals ($^{\bullet}$OH), electron holes (h^+), and superoxide radicals ($O_2^{\bullet-}$), respectively, on the surface of the Ag-doped ZnO NPs. When the reaction was carried out in the absence of scavengers, ~95% MG dye degradation was recorded. However, photocatalysis in the presence of BQ, TB, and AO accounted for ~41%, ~78%, and ~84% MG dye degradation, respectively (Fig. 13). These experiments showed that ROS play an important role in the degradation of MG dye.

4.   Mechanism of Ag-doped ZnO assisted photocatalytic degradation of MG dye

The proposed mechanism of the photocatalytic degradation of MG dye under visible light is presented in Fig. 14. It was observed that the ZnO NPs have a large band gap owing to their small size, and consequently, higher energy is required to excite electrons from the VB to the CB.[68] The photoexcitation of electrons generated equivalent holes in the VB, which, together with electrons, tended to recombine, reducing the efficiency of photocatalytic dye degradation (PDD).[68] However, the addition of noble metals into semiconductor photocatalysts can prevent

such recombination events, thereby improving the overall efficiency of PDD.[69] In one such approach, the Ag-doped ZnO NPs facilitate effective PDD by generating ROS. The Schottky barrier at the interface of the Ag-doped ZnO NPs, where the Fermi level energy of Ag is lower than the CB of pure ZnO, facilitates the transfer of electrons from ZnO to Ag.[70,71] These electrons react with absorbed O_2 and produce superoxide radical ($O_2^{\bullet-}$) anions, and the photoexcited holes in the VB can oxidize H_2O and OH groups to produce hydroxyl radicals ($^{\bullet}$OH) that are capable of degrading the dye molecules.

5.   Antibacterial activity of pure and Ag-doped ZnO NPs

The antibacterial activity of pure and Ag-doped ZnO NPs was investigated against *E. coli*. *E. coli* is a Gram negative, rod-shaped, facultative anaerobic bacterium that belongs to the family *Enterobacteriaceae*.[72] This bacterium is methyl red positive and gives negative oxidase, citrate, and Voges–Proskauer results.[73] *E. coli* is reported to cause various water-borne diseases in humans,[74] and its presence in water indicates fecal contamination.[75]

The present study tested different doses of pure and Ag-doped ZnO NPs against *E. coli*. The NPs in all the treatments showed antibacterial activity in a dose-dependent manner.[76] The antibacterial activity of pristine ZnO NPs was lower than that of the Ag-doped ZnO NPs (shown in Fig. 15).[77,78]
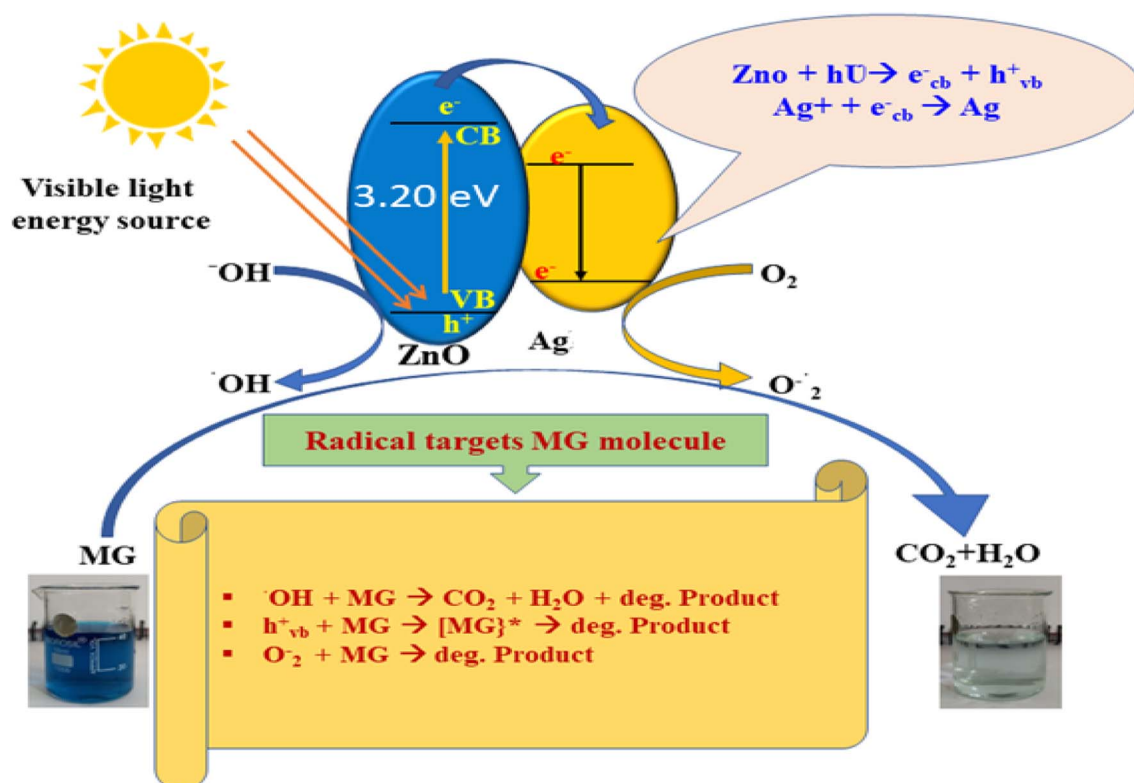

Fig. 14   Proposed mechanism of the photocatalytic degradation of MG dye in the presence of Ag-doped ZnO NPs.
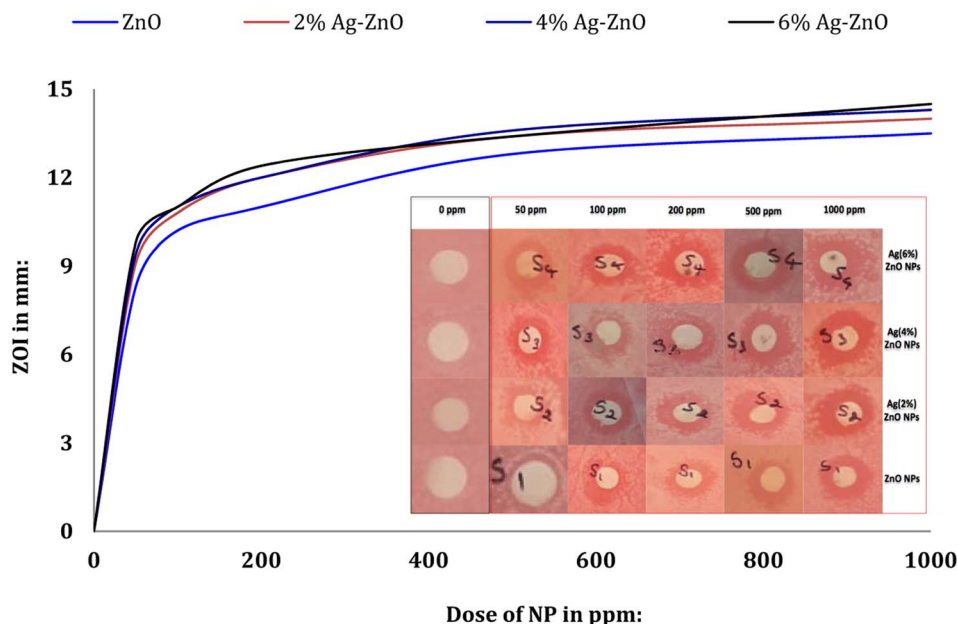
Fig. 15 Antibacterial properties of the Ag-doped ZnO NPs against *E. coli* (inset: ZOIs appeared after the NP treatments).

This could be due to the reduced size of the Ag-doped ZnO NPs (~36–38 nm) compared to the undoped ZnO NPs (~42 nm). These observations are in agreement with the findings of Talari *et al.*[79] It is assumed that with the reduction in the ZnO particle size, the number of ZnO NPs increases per unit volume of the nanopowder, resulting in higher surface area and increased levels of oxidizing agents (such as H_2O_2).[80] There was not much variation in the ZOI values in the case of treatment with the ZnO NPs doped with 2 to 6 wt% Ag. Overall, 1000 ppm was the most inhibitory dose for the growth of *E. coli*, where ZOI values of
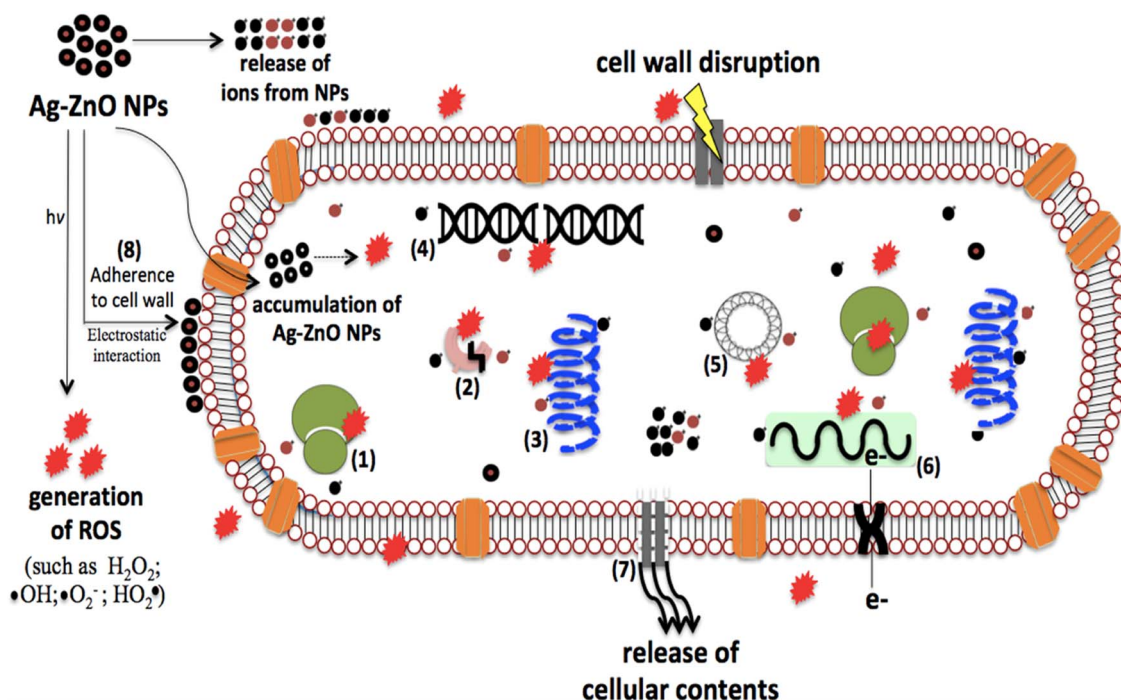
Fig. 16 Schematic of the mechanisms of antibacterial effects induced by Ag-doped ZnO NPs ((1): disassembly of ribosomes; (2): inhibition of enzymatic activity; (3): protein denaturation; (4): genomic DNA damage and inhibition of replication; (5): inhibition of plasmid DNA replication; (6): mitochondrial dysfunction, which inhibits respiratory enzymes and electron transport; (7): leakage in the bacterial cell membrane; (8): alteration of permeability and disruption of the integrity of the cell membrane).

≥14 mm were recorded for the Ag-doped ZnO NPs. The ZOI value for undoped ZnO NPs at 1000 ppm was similar to those recorded at 500 ppm for Ag-doped ZnO NPs, and at this concentration (500 ppm) the maximum ZOI was observed for the 4 wt% Ag-doped ZnO NPs. The three plausible routes of ZnO toxicity to the microbes are (i) ROS generation, (ii) the release of Zn^{2+} ions in aqueous media, and (iii) electrostatic interaction with the cell wall,[81] which are shown in Fig. 16. The overall effects of these routes on a bacterial cell will be DNA and protein disruption, membrane damage, cellular fluid leakage, and enzyme deactivation.[81]

Doping of metals in ZnO nanostructures enhance the photoexcitation efficiency, photocatalytic and antimicrobial activities.[81] In the present work, we used Ag as a dopant metal, which, in addition to modifying the optical and catalytic properties of ZnO, exhibits intrinsic antimicrobial activity against a diverse range of pathogenic bacteria.[81] Sharma et al.[80] recorded similar observations, where an increase in Ag metal dopant concentration and decrease in CS of ZnO NPs offered higher antibacterial activity against *S. aureus*. Talari et al.[79] also cited similar findings against *E. coli*.

6. Conclusion

In the current study, we fabricated ZnO NPs doped with different concentrations of Ag, and investigated their catalytic, photocatalytic and antimicrobial properties. The Ag-doped ZnO NPs show higher photocatalytic activity than pure ZnO NPs in the photodegradation of MG dye. The 4 wt% Ag-doped ZnO NPs as a catalyst (5 mg loading) degraded ∼95% MG dye (80 mg L^{-1} dye) within 1.5 h at neutral pH under visible light conditions. The results were also promising (∼85% dye degradation in 4 h) under dark conditions using the 4 wt% Ag-doped ZnO NPs without changing the other reaction conditions. This study provides a nanocatalyst that is capable of treating wastewater efficiently, is re-useable for multiple treatment cycles and is able to treat waste water under both visible light and dark conditions. In the antimicrobial investigation, the nanocatalyst provided a remarkable ZOI at a minimal concentration of 50 µg mL^{-1} against prominent faecal coliform in domestic wastewater, *i.e.*, *E. coli*, in a dose-dependent manner. Further, this investigation may inspire the development of more futuristic robust platforms based on functionalized metal oxide nanostructures for wastewater treatment.

Author contributions

Sagar Vikal: experimental work, conception, analysis and interpretation of data, writing the manuscript. Yogendra K. Gautam: conception, design of the experiments, interpretation of data, drafting of the manuscript. Swati Meena: experimental work, drafting manuscript. Vijay Parewa: design of the experiments, interpretation of data, drafting of the manuscript. Ashwani Kumar: the acquisition of data, analysis and interpretation of data. Ajay Kumar: experimental work, the acquisition of data and the drafting of the manuscript. Sushila Meena: the

acquisition of data. Sanjay Kumar: drafting of the manuscript. Beer Pal Singh: analysis of data and the drafting of the manuscript.

Conflicts of interest

The authors declare that there are no conflicts of interest.

References

1 Y. Cui, Q. Ma, X. Deng, Q. Meng, X. Cheng, M. Xie, X. Li, Q. Cheng and H. Liu, *Appl. Catal., B*, 2017, **206**, 136–145.

2 D. Bhatia, N. R. Sharma, J. Singh and R. S. Kanwar, *Crit. Rev. Environ. Sci. Technol.*, 2017, **47**, 1836–1876.

3 H. Sun, Z. Yang, Y. Pu, W. Dou, C. Wang, W. Wang, X. Hao, S. Chen, Q. Shao, M. Dong, S. Wu, T. Ding and Z. Guo, *J. Colloid Interface Sci.*, 2019, **547**, 40–49.

4 D. Bhatia, N. Sharma, J. Singh and R. Kanwar, *Crit. Rev. Environ. Sci. Technol.*, 2017, **47**, 1836–1876.

5 M. Moradi, G. Moussavi, K. Yaghmaeian, A. Yazdanbakhsh, V. Srivastava and M. Sillanpää, *Appl. Catal., B*, 2020, **260**, 118128.

6 M. Ali, S. Sharif, S. Anjum, M. Imran, M. Ikram, M. Naz and S. Ali, *Mater. Res. Express*, 2019, **6**, 1250d5.

7 M. Shariati, A. Samadi-Maybodi and A. Colagar, *J. Mater. Chem. A*, 2018, **6**, 20433.

8 J. Lim, S. S. Goh, S. S. Liow, K. Xue and X. J. Loh, *J. Mater. Chem. A*, 2019, **7**, 18759–18791.

9 S. Li, S. Silvers and M. Samy El-Shall, *MRS Proc.*, 1996, 452.

10 S. Vikal, Y. Gautam, A. Ambedkar, D. Gautam, J. Singh, D. Pratap, A. Kumar, S. Kumar, M. Gupta and B. Singh, *J. Semicond.*, 2022, **43**, 032802.

11 S. Moeen, M. Ikram, A. Haider, J. Haider, A. Ul-Hamid, W. Nabgan, T. Shujah, M. Naz and I. Shahzadi, *ACS Omega*, 2022, **7**, 46428–46439.

12 T. Pathak, R. Kroon, V. Craciun, M. Popa, M. Chifiriuc and H. Swart, *Heliyon*, 2019, **5**, e01333.

13 S. Mishra, U. Tripathi, R. Kumar and R. Shukla, *Mater. Lett.*, 2022, **308**, 131242.

14 M. Rabbani, J. Shokraiyan, R. Rahimi and R. Amrollahi, *Water Sci. Technol.*, 2021, **84**, 1813–1825.

15 A. Ambedkar, M. Singh, V. Kumar, V. Kumar, B. Singh, A. Kumar and Y. Gautam, *Surf. Interfaces*, 2020, **19**, 100504.

16 K. Karthik, A. Raghu, K. Reddy, R. Ravishankar, M. Sangeeta, N. Shetti and C. Reddy, *Chemosphere*, 2022, **287**, 132081.

17 O. Zelekew, P. Fufa, F. Sabir, D. Andoshe, N. Gultom, H. Abdellah, D. Kuo, X. Chen and G. Devulapalli, *J. Nanomater.*, 2022, **2022**, 1–10.

18 S. Liu, L. Zhu, W. Cao, P. Li, Z. Zhan, Z. Chen, X. Yuan and J. Wang, *J. Alloys Compd.*, 2021, **858**, 157654.

19 X. Zhu, J. Wang, D. Yang, J. Liu, L. He, M. Tang, W. Feng and X. Wu, *RSC Adv.*, 2021, **11**, 27257–27266.

20 M. Ikram, H. Shahid, J. Haider, A. Haider, S. Naz, A. Ul-Hamid, I. Shahzadi, M. Naz, W. Nabgan and S. Ali, *ACS Omega*, 2022, **7**, 39347–39361.

21 M. Mishra and D. Chun, *Appl. Catal., A*, 2015, **498**, 126–141.

22 M. Kadhim, M. Mahdi, J. Hassan and A. Al-Asadi, *Nanotechnology*, 2021, **32**, 195706.

23 S. Kumar, V. Singh and A. Tanwar, *J. Mater. Sci.: Mater. Electron.*, 2015, **27**, 2166–2173.

24 M. Ikram, R. Murray, M. Imran, S. Ali and S. I. Shah, *Mater. Res. Bull.*, 2016, **75**, 35–40.

25 S. Hosseini, I. Sarsari, P. Kameli and H. Salamati, *J. Alloys Compd.*, 2015, **640**, 408–415.

26 A. Dandia, V. Parewa and K. Rathore, *Catal. Commun.*, 2012, **28**, 90–94.

27 A. Dandia, S. Bansal, R. Sharma, D. Kumar Mahawar, K. Rathore, M. Lal Meena and V. Parewa, *J. Photochem. Photobiol., A*, 2020, **389**, 112242.

28 A. Dandia, V. Parewa, S. Gupta and K. Rathore, *J. Mol. Catal. A: Chem.*, 2013, **373**, 61–71.

29 C. Jaramillo-Páez, J. Navío, M. Hidalgo and M. Macías, *Catal. Today*, 2018, **313**, 12–19.

30 X. Zhu, J. Wang, D. Yang, J. Liu, L. He, M. Tang, W. Feng and X. Wu, *RSC Adv.*, 2021, **11**, 27257–27266.

31 R. Zeferino, M. Flores and U. Pal, *J. Appl. Phys.*, 2011, **109**, 014308.

32 L. Yousif, N. Ibrahim, R. Kamel and M. Rahmah, *IOP Conf. Ser.: Earth Environ. Sci.*, 2022, **961**, 012016.

33 A. Kadam, R. Dhabbe, A. Gophane, T. Sathe and K. Garadkar, *J. Photochem. Photobiol., B*, 2016, **154**, 24–33.

34 L. Armijo, S. Wawrzyniec, M. Kopciuch, Y. Brandt, A. Rivera, N. Withers, N. Cook, D. Huber, T. Monson, H. Smyth and M. Osiński, *J. Nanobiotechnol.*, 2020, 18.

35 M. Adil, T. Khan, M. Aasim, A. Khan and M. Ashraf, *AMB Express*, 2019, **9**, 1–12.

36 S. Schrey, E. Erkenbrack, E. Früh, S. Fengler, K. Hommel, N. Horlacher, D. Schulz, M. Ecke, A. Kulik, H. Fiedler, R. Hampp and M. Tarkka, *BMC Microbiol.*, 2012, 12.

37 R. Kumar, A. Umar, G. Kumar and H. Nalwa, *Ceram. Int.*, 2017, **43**, 3940–3961.

38 M. R. Shariati, A. Samadi-Maybodi and A. Hosseinzadeh Colagar, *J. Mater. Chem. A*, 2018, **6**, 20433.

39 L. Muñoz-Fernandez, A. Sierra-Fernandez, O. Milošević and M. Rabanal, *Adv. Powder Technol.*, 2016, **27**, 983–993.

40 H. Liu, H. Liu, J. Yang, H. Zhai, X. Liu and H. Jia, *Ceram. Int.*, 2019, **45**, 20133–20140.

41 M. Thomas and J. Cui, *J. Phys. Chem. Lett.*, 2010, **1**, 1090–1094.

42 M. Nie, J. Liao, H. Cai, H. Sun, Z. Xue, P. Guo and M. Wu, *Chem. Phys. Lett.*, 2021, **768**, 138394.

43 Y. Li, X. Zhao and W. Fan, *J. Phys. Chem. C*, 2011, **115**, 3552–3557.

44 S. AL-Jawad, S. Sabeeh, A. Taha and H. Jassim, *J. Sol-Gel Sci. Technol.*, 2018, **87**, 362–371.

45 T. Ai, Y. Fan, H. Wang, X. Zou, W. Bao, Z. Deng, Z. Zhao, M. Li, L. Kou, X. Feng and M. Li, *Front. Chem.*, 2021, **9**, 661127.

46 C. Jaramillo-Páez, J. Navío, M. Hidalgo and M. Macías, *Catal. Today*, 2018, **313**, 12–19.

47 S. Sagadevan, K. Pal, Z. Chowdhury and M. Hoque, *J. Sol-Gel Sci. Technol.*, 2017, **83**, 394–404.

48 R. Zeferino, M. Flores and U. Pal, *J. Appl. Phys.*, 2011, **109**, 014308.

49 O. Yildirim, *Selcuk Univ. J. Eng., Sci. Technol.*, 2018, **6**, 632–642.

50 H. A. Habeeb Alshamsi and B. S. Hussein, *Orient. J. Chem.*, 2018, **34**, 1898–1907.

51 S. Hosseini, I. Sarsari, P. Kameli and H. Salamati, *J. Alloys Compd.*, 2015, **640**, 408–415.

52 Z. Kayani, F. Manzoor, A. Zafar, M. Mahmood, M. Rasheed and M. Anwar, *Opt. Quantum Electron.*, 2020, **52**, 1–18.

53 D. Arumai Selvan, M. keerthi, S. Murugesan, S. Shobana, B. Lakshmi, V. Veena and A. Rahiman, *Mater. Chem. Phys.*, 2021, **272**, 124903.

54 S. Kansal, M. Singh and D. Sud, *J. Hazard. Mater.*, 2007, **141**, 581–590.

55 E. M. Mostafa and E. Amdeha, *Environ. Sci. Pollut. Res.*, 2022, **29**, 69861–69874.

56 A. Amini Herab, D. Salari, A. Ostadrahimi and A. Olad, *J. Polym. Res.*, 2022, **29**, 321.

57 A. M. Rabie, M. R. Abukhadra, A. M. Rady, S. A. Ahmed, A. Labena, H. S. H. Mohamed, M. A. Betiha and J. J. Shim, *Res. Chem. Intermed.*, 2020, **46**, 1955–1973.

58 J. Yang, X. Xu, Y. Liu, Y. Gao, H. Chen and H. Li, *Colloids Surf., A*, 2019, **582**, 123858.

59 R. J. Kamble, P. V. Gaikwad, K. M. Garadkar, S. R. Sabale, V. R. Puri and S. S. Mahajan, *J. Iran. Chem. Soc.*, 2022, **19**, 303–312.

60 N. Chauhan, V. Singh, S. Kumar, M. Kumari and K. Sirohi, *J. Mol. Struct.*, 2019, **1185**, 219–228.

61 V. Eskizeybek, F. Sarı, H. Gülce, A. Gülce and A. Avcı, *Appl. Catal., B*, 2012, **119**, 197–206.

62 M. Bahal, N. Kaur, N. Sharotri and D. Sud, *Adv. Polym. Technol.*, 2019, 1–9.

63 K. Sirohi, S. Kumar, V. Singh, N. Chauhan and A. Vohra, *Mater. Res. Express*, 2019, **6**, 075901.

64 C. Hachem, F. Bocquillon, O. Zahraa and M. Bouchy, *Dyes Pigm.*, 2001, **49**, 117–125.

65 M. Barjasteh-Moghaddam and A. Habibi-Yangjeh, *J. Iran. Chem. Soc.*, 2011, **8**, S169–S175.

66 A. Dandia, S. Gupta, V. Parewa, A. Sharma, K. Rathore and A. Sharma, *Tetrahedron Lett.*, 2013, **54**, 5711–5717.

67 B. Divband, M. Khatamian, G. Eslamian and M. Darbandi, *Appl. Surf. Sci.*, 2013, **284**, 80–86.

68 A. Kadam, R. Dhabbe, A. Gophane, T. Sathe and K. Garadkar, *J. Photochem. Photobiol., B*, 2016, **154**, 24–33.

69 C. An, S. Wang, Y. Sun, Q. Zhang, J. Zhang, C. Siu, C. Wang and J. Fang, *J. Mater. Chem. A*, 2015.

70 Y. Xu, S. Wu, X. Li, H. Meng, X. Zhang, Z. Wang and Y. Han, *Chem. Phys. Lett.*, 2017, **679**, 119–126.

71 J. Tolia, M. Chakraborty and Z. Murthy, *Pol. J. Chem. Technol.*, 2012, **14**, 16–21.

72 P. Desmarchelier and N. Fegan, *Encyclopedia of Dairy Sciences*, 2002, pp. 948–954.

73 C. Batt, *Encyclopedia of Food Microbiology*, 2014, pp. 688–694.

74 S. Percival and D. Williams, *Microbiology of Waterborne Diseases*, 2014, pp. 89–117.

75 E. Anastasi, B. Matthews, H. Stratton and M. Katouli, *Appl. Environ. Microbiol.*, 2012, **78**, 5536–5541.

76 F. H. Dowlatababdi, G. Amiri and M. M. Sichani, *Nanomed. J.*, 2017, **4**(1), 50–54.

77 A. Chauhan, R. Verma, S. Kumari, A. Sharma, P. Shandilya, X. Li, K. Batoo, A. Imran, S. Kulshrestha and R. Kumar, *Sci. Rep.*, 2020, 10.

78 S. Sampath, M. Bhushan, V. Saxena, L. Pandey and L. Singh, *Mater. Technol.*, 2022, 1–10.

79 M. Talari, A. Abdul Majeed, D. Tripathi and M. Tripathy, *Chem. Pharm. Bull.*, 2012, **60**, 818–824.

80 N. Sharma, J. Kumar, S. Thakur, S. Sharma and V. Shrivastava, *Drug Invent. Today*, 2013, **5**, 50–54.

81 M. Carofiglio, S. Barui, V. Cauda and M. Laurenti, *Appl. Sci.*, 2020, **10**, 5194.